Experimental and Cubic Plus Association Equation of State modelling study of phase equilibria of 1-Ethyl-3-methylimidazolium methanesulfonate + methanol + dimethyl carbonate + water binary and quaternary mixtures

The role of ionic liquids vapor pressure in modelling

Laakso, Juho Pekka; Asadzadeh, Behnaz; Uusi-Kyyny, Petri; Liang, Xiaodong; Kontogeorgis, Georgios M.; Alopaeus, Ville

Published in:
Journal of Molecular Liquids

Link to article, DOI:
10.1016/j.molliq.2024.126775

Publication date:
2025

Document Version
Publisher's PDF, also known as Version of record

Journal of Molecular Liquids 422 (2025) 126775

Contents lists available at ScienceDirect

Journal of Molecular Liquids

journal homepage: www.elsevier.com/locate/molliq

Experimental and Cubic Plus Association Equation of State modelling study of phase equilibria of 1-Ethyl-3-methylimidazolium methanesulfonate + methanol + dimethyl carbonate + water binary and quaternary mixtures: The role of ionic liquids vapor pressure in modelling

Juho-Pekka Laakso [a,*], Behnaz Asadzadeh [a], Petri Uusi-Kyyny [a], Xiaodong Liang [b], Georgios M. Kontogeorgis [b], Ville Alopaeus [a]

[a] Aalto University, School of Chemical Technology, Department of Chemical and Metallurgical Engineering, P.O. Box 16100, FI-00076 Aalto, Finland
[b] Center for Energy Resources Engineering (CERE), Department of Chemical and Biochemical Engineering, Technical University of Denmark, DK2800 Kgs, Lyngby, Denmark

ARTICLE INFO

Keywords:
Ionic liquids
Phase equilibria
Binary mixtures
Quaternary mixtures
Cubic plus association
Ionic liquids vapor pressure

ABSTRACT

Understanding the phase equilibria of ionic liquids (ILs) in mixtures related to dimethyl carbonate (DMC) synthesis is important for enhancing the yield of DMC by absorbing the water produced during the reaction. 1-Ethyl-3-methylimidazolium methanesulfonate ([Emim][$MeSO_3$]) shows promise as a water absorbent for this application.

This study investigates the phase equilibria of binary and quaternary mixtures containing [Emim][$MeSO_3$], water, methanol, and DMC at 102 kPa. Vapor-liquid equilibrium (VLE) and liquid-liquid equilibrium (LLE) were measured using the circulation still and cloud point method. The Cubic Plus Association (CPA) equation of state (EOS) was used for modelling, using two parameterization strategies for [Emim][$MeSO_3$]. The first strategy used density and vapor pressure (CPAρP), whereas the second strategy used density and isobaric heat capacity (CPAρC).

The CPAρP parameter set demonstrated generally higher accuracy in modelling binary and quaternary mixtures. It slightly improved VLE modelling of the H_2O + [Emim][$MeSO_3$] mixture and enhanced LLE modelling of DMC + [Emim][$MeSO_3$] mixture over the CPAρC parameter set, with AAD values of 0.01 and 0.12 for the mole fraction of [Emim][$MeSO_3$]. For the quaternary mixture, the CPAρP parameter set outperformed the CPAρC parameter set in modelling the relative volatility of methanol with AAD values of 0.11 and 0.17.

The results provide insights into phase equilibria modelling for mixtures involving [Emim][$MeSO_3$], water, methanol, and DMC. Including the vapor pressure of [Emim][$MeSO_3$] in the parameter regression improved the accuracy of the CPA model enhancing its ability to realistically simulate phase equilibria, which is essential for designing water absorbent for DMC synthesis.

1. Introduction

The possibility of converting CO_2 into value-added products has garnered attention due to global warming. One promising opportunity is the synthesis of dimethyl carbonate (DMC) from CO_2 and methanol. DMC can be used in many applications, such as fuel additives and building block reagent [1]. However, DMC yield is limited by the thermodynamic barrier which can be overcome by absorbing water and thus shifting the chemical equilibrium toward products [2]. Ionic liquids (ILs) can be tailored to have hydrophilic or hydrophobic properties [3], making them promising candidates for shifting the chemical equilibrium in the direct synthesis of DMC by absorbing the water produced during the reaction. Among ILs, [Emim][$MeSO_3$] shows particular potential as a water absorbent due to its high affinity towards water [4,5].

ILs are composed of cations and anions with a melting point below 100°C. They have garnered significant interest within the scientific community [6] due to their unique properties, including high thermal and chemical stability and negligible vapor pressure. Their properties can be tailored by changing the combination of cations and anions [7].

* Corresponding author.
E-mail address: juho-pekka.laakso@aalto.fi (J.-P. Laakso).

https://doi.org/10.1016/j.molliq.2024.126775
Received 6 September 2024; Received in revised form 2 December 2024; Accepted 20 December 2024
Available online 25 December 2024

Nomenclature

Acronyms

AARD%	Average absolute relative deviation
AAD	Average absolute deviation
EOS	Equation of State
SRK	Soave-Redlich-Kwong
CPA	Cubic Plus Association
e-CPA	electrolyte Cubic Plus Association
PC-SAFT	Perturbed Chain Statistical Associating Fluid Theory
e-PC-SAFT	electrolyte Perturbed Chain Statistical Associating Fluid Theory
COSMO-RS	Conductor-like Screening Model for Real Solvents
NRTL	Non-Random Two-Liquid
IL	Ionic liquid
OF	Objective function
VLE	Vapor-Liquid Equilibrium
LLE	Liquid-Liquid Equilibrium
GC	Gas-Chromatography
TXY	Temperature-Composition phase diagram
PXY	Pressure-Composition phase diagram
xy	Liquid-vapor composition diagram
CAS	Chemical Abstracts Service registry number
[Emim][$MeSO_3$]	1-Ethyl-3-methylimidazolium methanesulfonate
H_2O	Water
MeOH	Methanol
DMC	Dimethyl carbonate
PrOH	2-Propanol
CO_2	Carbon dioxide

English letters

a	Energy Parameter
a_0	Parameter in the Energy Term
b	Co-volume parameter
c_1	Parameter in energy term
Γ	Reduced energy parameter
u	Standard uncertainty
$g(\rho)$	Radial Distribution Function
k	Binary interaction parameter
T	Temperature
Tr	Reduced temperature
P	Pressure
Cp	Isobaric heat capacity
R_g	Gas constant
x_i	Liquid phase mole fraction of component i
X_A	Mole Fraction of the Component not Bonded at Site A
y_i	Vapor phase mole fraction of component i
v_m	Molar volume
F	Response factor
A	Surface area of GC-signal

Greek letters

α_{12}	Relative volatility between components 1 and 2
ε	Association energy parameter
β	Association volume parameter
Δ_{AiBj}	Association Strength of Interaction Between Sites A and B
ρ	Molar density
γ	Activity coefficient

subscripts

A, B	Sites A, B on the molecule
Std	Standard
Sat	Saturation state
i , j	Component i and j

superscripts

exp	Experimental values
cal	Calculated values

As a result, ILs have potential applications as CO_2 absorbents and as a solvent for the dissolution of cellulose [7-9]. Recently, they have been applied to advanced materials, such as in solar cells and nanoreactors [10]. Although ILs are often referred to as green solvents due to their low vapor pressures, their toxicity has drawn attention, which contradicts this classification [11].

One IL that has garnered interest is [Emim][$MeSO_3$], due to its strong interaction with water, relatively high thermal stability, and low viscosity, making it a promising candidate for drying gases [4]. The mixture of [Emim][$MeSO_3$] and H_2O is also scientifically interesting. A phase equilibria study indicates that the interaction between H_2O molecules is surpassed by the interaction between [Emim][$MeSO_3$] and H_2O, which explains the hygroscopicity of [Emim][$MeSO_3$] [5]. Moreover, another study suggests that [Emim][$MeSO_3$] forms a non-polar aggregation structure even in the presence of a high quantity of H_2O [12].

Various thermodynamic models have been used to model phase equilibria in mixtures involving ILs. Activity coefficient models like UNIFAC [13], NRTL [14,15], and quantum chemistry approaches such as COSMO-RS [16] have been applied to model phase equilibria in mixtures containing ILs. Additionally, the equation of state (EOS) models that include the association term, such as the CPA [17] and PC-SAFT [18], have been applied in modelling phase equilibria of mixtures that involve polar components [19] and ILs [20-22]. Electrolyte EOS models, such as the e-CPA [23] and e-PC-SAFT [24,25], are also effective modelling options for IL mixtures [26-29]. Since the behavior of ILs can be considered as solvated ions (weak salt) in their pure form [30], EOS models with the association term are a suitable choice alongside electrolyte EOS models.

ILs are described as neutral pairwise ions, and complex interactions within ILs are simplified to an association interaction in the association EOS models [31,32]. The choice of the association scheme is necessary for these EOS models [33,34]. Typically, the 2B association scheme has been successfully applied for modelling phase equilibria with the CPA [20,21,35]. Additionally, the association scheme has been determined from the number of lone-pair electrons in anion for the PC-SAFT model [36].

The association term in the CPA or PC-SAFT is essential when modelling the phase equilibria of the H_2O-IL mixtures, due to the complex nature of these systems [37]. The CPA has been used to model LLE in mixtures involving hydrophobic ILs ([Emim][NTf_2] and [Bmim][NTf_2]) and water [20]. In contrast, PC-SAFT has been used to model VLE in mixtures of H_2O and ILs [22]. The pure component parameters for PC-SAFT were regressed using density, VLE, and infinite dilution activity coefficient data. Interestingly, the regression resulted in a value of 0 for the association energy parameter (ε) for most of the studied ILs. This was explained by the possibility that H_2O surrounds IL molecules, preventing self-association between IL molecules.

The main objective of this work is to study the effect of IL vapor pressure on the CPA model capability in modelling phase equilibria in mixtures related to DMC synthesis. It is generally unclear which properties should be used to regress pure component parameters for ILs in the CPA model to obtain optimal parameters. This challenge also extends to simpler components. The vapor pressure generally appears to be essential for parameter regression [19]. The CPA model generally uses density and vapor pressure data in pure component parameter

regression [38]. Due to the lack of experimental data on IL vapor pressure, derivative properties such as isobaric heat capacity [21,35] and speed of sound [39] are commonly used to regress the pure component parameters for ILs in the CPA model. However, only a minimal number of CPA and PC-SAFT parameters use the ILs vapor pressure in the regression [20,40].

ILs have exceptionally low vapor pressures and are often unavailable for CPA parameter regression. Typically, vapor pressure data is important for identifying CPA pure component parameters. However, the impact of IL vapor pressure on CPA parameters and phase equilibrium modelling has received little attention. Thus, the novelty of this work lies in understanding the effect of IL vapor pressure on CPA parameterization and phase equilibrium modelling for highly polar binary and quaternary mixtures.

This study focuses on the experimental phase equilibria of binary and quaternary mixtures involving [Emim][$MeSO_3$] + H_2O + MeOH + DMC and capabilities of the CPA for modelling phase equilibria with two different parameter optimization strategies. Section 2 presents the experimental work for VLE and LLE with density measurements. This also includes validating the VLE measurements with thermodynamic consistency tests for the MeOH + DMC mixture. The modelling approach used in this work (the CPA) is presented in Section 3. Experimental and modelling results are in Section 4 and Section 5 includes the conclusion drawn from this work.

2. Experiments

We measured the VLE for binary mixtures (H_2O + [Emim][$MeSO_3$] and MeOH + [Emim][$MeSO_3$]) and a quaternary mixture (MeOH + DMC + H_2O + [Emim][$MeSO_3$]), while the LLE was measured for the DMC + [Emim][$MeSO_3$] mixture. It was observed that the [Emim][$MeSO_3$] formed two liquid phases with DMC, while it was completely soluble in both H_2O and MeOH. All components were completely miscible in the quaternary mixture for which the VLE measurements were obtained.

2.1. Materials

All used materials and their specifications are shown in Table 1. [Emim][$MeSO_3$] was dried in a vacuum at 60 °C for 2 days before each experiment. The H_2O content of [Emim][$MeSO_3$] was determined using Karl-Fischer titration after vacuum drying, and [Emim][$MeSO_3$] was stored in a desiccator during the experiments. For all our calculations regarding the experiments, the H_2O content of [Emim][$MeSO_3$] was considered. The purity of [Emim][$MeSO_3$] was specified in the certificate of analysis provided by the supplier.

2.2. Vapor-Liquid equilibria measurements

The vapor-liquid equilibrium of the binary and quaternary mixtures was measured using a modified Yerazunis-type circulation still [41]. In general, this apparatus functions as follows. The apparatus creates flows for the liquid and vapor phases between the boiler, equilibrium chamber, condenser, and the sampling chambers. The vapor-liquid equilibrium is achieved in the equilibrium chamber followed by the vapor and liquid phase separation. After this, condensed vapor and liquid phases are collected in two separate sampling chambers to obtain measured samples. Fluid flows from these chambers to the reboiler, vaporizing the mixture after which returns to the equilibrium chamber [15,42].

In our experiments, the temperature of the boiling mixture was measured with a calibrated ALS F200 thermometer (Tempcontrol, Netherlands) with a Pt-100 temperature probe. Similarly, the pressure of the circulation still was followed with a calibrated pressure transducer (PMP 4070, Druck). Samples for each mixture were obtained from the sampling chambers after letting the circulation still stabilize for a minimum of 30 minutes. These samples were taken with a syringe and diluted with propanol for composition samples. The mass of each sample and propanol was measured with an ES 520A balance (Precisa, Switzerland).

The composition of the VLE samples was measured using an Agilent 7890 gas chromatograph (GC). The GC parameters are provided in Table S1. The composition was calculated using the response factors as shown in Equation (1). These factors were determined for MeOH, DMC, and H_2O, while 2-propanol (PrOH) was used as an internal standard.

$$F_i = F_{std}\frac{A_{std}}{A_i}\frac{m_i}{m_{std}} \tag{1}$$

where F_i is the response factor for component i, F_{std} is the response factor of the internal standard (2-Propanol), which is set to 1, A_{std} and A_i are surface area of GC signal for the internal standard, and component i, m_{std} and m_i are masses for internal standard and component i. The response factor for each component was calibrated for 8 mixtures. The mole fractions for each sample were calculated using the response factors for MeOH, DMC, and H_2O, while mole fractions of [Emim][$MeSO_3$] were obtained by subtracting mole fractions of MeOH, DMC, and H_2O from 1.

The standard uncertainties for each measurement were evaluated according to guidelines [43]. The standard uncertainty for temperature $u(T)$ was 0.02 K for the DMC + MeOH mixture. However, the uncertainty of the temperature increased at higher temperatures, ranging from 0.05 to 1.4 K. This might be due to heat loss in the circulation still apparatus. The standard uncertainty for mole fraction was $u(x) = u(y) = 0.005$ for the binary mixtures. For the quaternary mixtures, the composition uncertainty increased to $u(x) = u(y) = 0.01$. The standard uncertainty for pressure $u(P)$ remained constant at 0.2 kPa for all mixtures.

2.3. Liquid-Liquid equilibria measurements

The liquid-liquid equilibrium was measured for the DMC + [Emim][$MeSO_3$] mixture with the cloud point method described in previous work [44]. Measurements were conducted in a glass vessel (volume = 50 cm^3) with a jacket thermostat in which water circulates at a controlled temperature and the mixture is stirred with a magnetic stirrer. A thermostat (Lauda E200) was utilized for controlling the temperature with a standard uncertainty of $u(T) = 0.2$ K and the composition of mixture was determined with mass basis using a Precisa 410 AM-FR balance with a standard uncertainty of $u(m) = 0.002$ g. The cloud point measurements were conducted for a constant amount of [Emim][$MeSO_3$] and by increasing the temperature for the liquid-liquid split to disappear. After that, a known amount of DMC was added to form the two phases with a new temperature.

Table 1
Material used in this work and their purity.

Component	CAS number	Supplier	Purity	Water content mass fraction	Drying method
1-Ethyl-3-methylimidazolium methanesulfonate	145022-45-3	Merck	98.8%	0.009[a]	Vacuum drying
Water	7732-18-5		0.05 μS/cm (Type 1)		
Methanol	67-56-1	Merck	≥ 99.9%	0.0001[a]	Molecular sieves
Dimethyl carbonate	616-38-6	Merck	≥ 99%	Undetectable[a]	Molecular sieves
2-Propanol	67-63-0	Honeywell	≥ 99.9%	Undetectable[a]	Molecular sieves

a = Determined by Karl Fisher titration

2.4. Density measurements

Density was measured using a vibrating-tube Anton Paar DMA 5000 DMA HP high-pressure unit. The density measurements were taken after the temperature stabilized (after 15 min). Five measurements were taken at each temperature. The standard uncertainties for density, temperature, and pressure were $u(\rho) = 0.01$ kg/m^3, $u(T) = 0.05$ K, and $u(P) = 0.4$ kPa. The contribution of impurities to the uncertainty of the density measurements in [Emim][$MeSO_3$] was also considered [45]. The density measurements were taken from the freshly dried samples.

3. The CPA equation of state

The CPA equation of state [17] combines the well-known Soave-Redlich-Kwong equation of state (SRK) [46] with the association term from the work of Wertheim. Originally, the CPA is designed to handle multicomponent and multiphase mixtures with association or polar components in a simpler way than the use of the full SAFT theories. The CPA has similarities with SAFT theories since they both share similar association term from Wertheim's theory. The CPA can be expressed with Eqs. (2)–(5) [34].

$$P = \frac{R_g T}{V_m - b} - \frac{a(T)}{V_m(V_m + b)} - \frac{1}{2}\frac{R_g T}{V_m}\left[1 + \frac{1}{V_m}\frac{\partial ln g(\rho)}{\partial \rho}\right]\sum_i x_i \sum_{A_i}(1 - X_{A_i}) \quad (2)$$

where P = pressure, R_g = ideal gas constant, T = temperature, V_m is molecular volume, b is co-volume, g is the radial distribution function, ρ is the molar density, x_i is the mole fraction of component i and X_{Ai} is the key element in the association term which describes the fraction of sites A in compound i that does not form bonds with other active sites, calculable from Eq. (3).

$$X_{A_i} = \frac{1}{1 + \rho \sum_j x_j \sum_{B_j} X_{B_j} \Delta^{A_i B_j}} \quad (3)$$

where B_j = association site B in molecule j and Δ_{AiBj} = association strength. The association strength is calculated according to Eq. (4).

$$\Delta_{A_i B_j} = g(\rho)\left[exp\left(\frac{\varepsilon^{A_i B_j}}{R_g T}\right) - 1\right] b_{ij} \beta^{A_i B_j} \quad (4)$$

where $\varepsilon^{A_i B_j}$ = cross-association energy parameter and $\beta^{A_i B_j}$ = the cross-association volume parameter which represents the depth and width of the square well potential of the association interaction. Energy parameter $a(T)$ has a Soave-type temperature dependence as follows.

$$a(T) = a_0\left[1 + c_1\left(1 - \sqrt{T_r}\right)\right]^2 \quad (5)$$

where a_0 and c_1 are energy-related pure component parameters and T_r is the reduced temperature. In total, the CPA uses five parameters (three from the SRK EOS and two from the association term) and the CPA reduces to the SRK model in case of non-association compound.

To model mixtures with the CPA, specifying the mixing rule is necessary. Generally, the CPA utilizes the van der Waals one fluid mixing rule (vdW1f) for energy (Eq. (6)) and co-volume parameters (Eq. (7)).

$$a = \sum_i \sum_j x_i x_j a_{ij} \text{ where } a_{ij} = \sqrt{a_i a_j}(1 - k_{ij}) \quad (6)$$

where a_{ij} = cross energy parameter and k_{ij} = binary interaction parameter, which is constant and estimated from phase equilibria data. Co-volume parameter, according to the vdW1f rule, can be calculated as follows:

$$b = \sum_i \sum_j x_i x_j b_{ij} \text{ where } b_{ij} = \frac{b_i + b_j}{2} \quad (7)$$

where b_{ij} = cross co-volume parameter. For mixtures that contain two or more associating compounds, the combining rules are needed for $\varepsilon^{A_i B_j}$ and $\beta^{A_i B_j}$. The CR-1 combining rule is presented in Eq. (8).

$$\varepsilon^{A_i B_j} = \frac{\varepsilon^{A_i B_i} + \varepsilon^{A_j B_j}}{2}, \quad \beta^{A_i B_j} = \sqrt{\beta^{A_i B_i} \beta^{A_j B_j}} \quad (8)$$

4. Results and discussion

4.1. Experimental results

We measured the VLE of the MeOH + DMC mixture to validate the circulation still apparatus by comparing results to literature and conducting the thermodynamic consistency tests. The VLE results for this mixture are shown in Table 2, while the results are compared with literature [47,48] in Fig. 1. The results in Fig. 1 show that our experimental data are consistent with the literature values used for this comparison.

Two well-known thermodynamic consistency tests, the Herrington and Van Ness tests, were performed according to Kang et al. [49]. The Herrington test confirms that the mixture follows the Gibbs-Duhem equation across the full composition range. Thermodynamic consistency of the mixture is evaluated by calculating the surface area under the plot of $\ln(\gamma_1/\gamma_2)$ against x_1. The criterion for passing the Herrington test is described in detail elsewhere [49]. The Van Ness test validates that the NRTL activity coefficient model can accurately represent the VLE of the mixture. To pass the Van Ness test, the NRTL model must predict the bubble point pressure and vapor phase composition of VLE within 1% AARD. The VLE of the MeOH + DMC mixture measured in this work passed both the Herrington and Van Ness tests, and the results are presented in Table 3.

After confirming thermodynamic consistency, we measured the VLE of binary mixtures containing [Emim][$MeSO_3$]. Specifically, the boiling point temperature as a function of liquid and vapor compositions (TXY) was measured for H_2O + [Emim][$MeSO_3$] and MeOH + [Emim][$MeSO_3$] mixtures. The experimental results for H_2O + [Emim][$MeSO_3$] and MeOH + [Emim][$MeSO_3$] mixtures are shown in Tables 4 and 5. We measured the water content in the VLE experiment of MeOH + [Emim][$MeSO_3$] mixture, therefore Table 5 is reported as a ternary system. However, we consider this MeOH + [Emim][$MeSO_3$] as a binary mixture due to low enough water content. In both cases, the vapor phase composition contained primarily on H_2O or MeOH due to the negligible vapor pressure of [Emim][$MeSO_3$]. During the binary VLE measurements, we observed that the uncertainty of the temperature measurements increased at higher temperatures. This might be due to heat loss in

Table 2
Methanol (1) + DMC (2) vapor-liquid equilibrium measurements at 102 kPa.

T (K)	x_1	y_1
337.4	1.000	1.000
337.3	0.991	0.988
337.1	0.980	0.969
336.5	0.899	0.885
336.5	0.815	0.831
336.9	0.693	0.779
337.9	0.545	0.726
339.3	0.423	0.681
341.2	0.318	0.631
345.9	0.179	0.515
350.9	0.102	0.385
363.2	0.000	0.000

$u(x_1) = 0.005$, $u(y_1) = 0.005$, $u(T) = 0.1$ K, $u(P) = 0.2$ kPa.

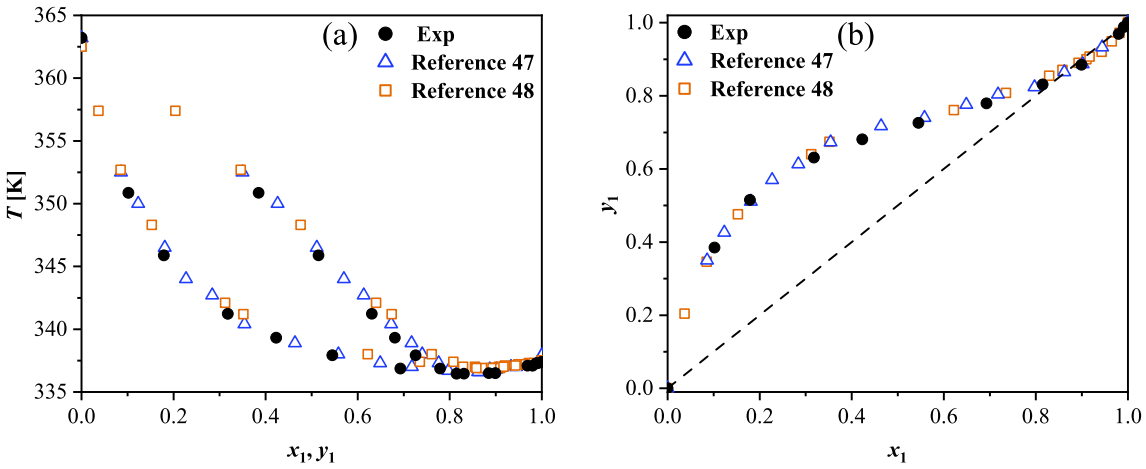

Fig. 1. Comparison of experimental VLE data for the MeOH (1) + DMC (2) mixture at 102 kPa. Our measurements are shown in Table 2, while other data is from literature [47,48]. (a) TXY-diagram, (b) xy-diagram.

Table 3
Calculated thermodynamic consistency test results for experimental VLE of MeOH + DMC mixture measured in this work. The criteria to pass the test are in parentheses.

	Herrington	Van Ness	
System	|D-J| (<10)	ΔP %(<1)	Δy %(<1)
MeOH-DMC	2.3	0.05	0.36

Table 4
VLE measurements of H_2O (1) + [Emim][$MeSO_3$] (2) at 102 kPa.

x_1	T(K)	$u(T)$/K
1.000	373.0	0.1
0.993	373.4	0.1
0.980	374.1	0.1
0.954	375.8	0.1
0.910	380.3	0.2
0.835	388.0	0.4
0.766	396.6	0.6
0.691	404.6	0.8
0.645	413.5	1.0
0.607	418.8	1.1
0.534	429.3	1.3
0.485	437.9	1.4

$u(x_1) = 0.005$, $u(P) = 0.2$ kPa.

Table 5
VLE measurements of MeOH (1) + H_2O (2) + [Emim][$MeSO_3$] (3) at 102 kPa.

x_1	x_3	T(K)	$u(T)$/K
1	0	337.7	0.1
0.951	0.034	338.8	0.1
0.911	0.074	340.5	0.1
0.842	0.142	344.8	0.3
0.787	0.195	349.7	0.5
0.700	0.280	355.1	0.7
0.585	0.391	368.5	1.1
0.459	0.520	382.0	1.3

$u(x_1) = 0.005$ $u(P) = 0.2$ kPa.

the circulation still apparatus at high temperatures. The LLE measurements for DMC + [Emim][$MeSO_3$] mixture are presented in Table 6. Additionally, the results of the [Emim][$MeSO_3$] density measurements are shown in Table S2.

We measured the VLE of the quaternary mixtures (MeOH + DMC+ H_2O +[Emim][$MeSO_3$] after measuring the VLE of the corresponding

Table 6
LLE measurements for DMC (1) + [Emim][$MeSO_3$] (2) at 101 kPa.

T(K)	x_1
293.2	0.539
303.2	0.543
313.2	0.547
323.2	0.558
333.2	0.562
343.2	0.573
353.2	0.578

$u(x) = 0.002$, $u(T) = 0.2$ K, $u(P) = 10$ kPa.

binary mixtures. The experimental data for the quaternary mixtures are shown in Tables S3-S14. The quaternary VLE measurements were performed by keeping the mole fraction of [Emim][$MeSO_3$] and H_2O roughly constant, while varying the mole fractions of MeOH and DMC. The TXY measurements for quaternary mixtures were conducted with roughly constant mole fractions of [Emim][$MeSO_3$] (≈ 0.05, ≈ 0.1, ≈ 0.2 and ≈ 0.3) and H_2O (≈ 0.1, ≈ 0.2 and ≈ 0.3). To describe the phase behavior of the quaternary mixture, the relative volatility of methanol (α_{12}) was calculated from the experimental data according to Eq. (9).

$$\alpha_{12} = \frac{(y_1/x_1)}{(y_2/x_2)} \tag{9}$$

where y_1 = methanol mole fraction in the vapor phase, x_1= methanol mole fraction in the liquid phase, y_2 = DMC mole fraction in the vapor phase and x_2 = DMC mole fraction in the liquid phase.

4.2. *Modelling results for the pure properties of [Emim][$MeSO_3$]*

The CPA pure component parameters are essential for modelling. We regressed these parameters for [Emim][$MeSO_3$], while pure component parameters for other compound are available in the literature [50]. These parameters are commonly obtained from density and vapor pressure data, the regression accuracy is typically within 1% AARD [38]. The AARD% and AAD are calculated according to Eqs. (10) and (11). However, these parameters have been regressed using vapor pressure data for ILs only in two studies [20,51].

We used two approaches to regress CPA pure component parameters for [Emim][$MeSO_3$]. In the first approach, we used density and vapor pressure data, while in the second, we used density and isobaric heat capacity data. The density data were measured in this work, while the saturated vapor pressure [52] and isobaric heat capacity [53] were

obtained from the literature. CPA pure component parameter regression was conducted in MATLAB by using a toolbox for parameter optimization [54]. Although, the fmincon method is commonly used for such regression, it was unsuitable for low vapor pressure data, as it often got stuck in a local minimum. Therefore, a method called GlobalSearch was employed, in which multiple initial points generated by its built-in algorithm were used together with fmincon. Additionally, the critical properties required for modelling were estimated for the [Emim][$MeSO_3$] using the Lydersen-Joback-Reid group contribution method [55].

We used the objective functions OF_1 and OF_2 from Eqs. (12) and (13) for parameter regression. A weight factor of 0.05 was applied to vapor pressure in OF_1 due to the high uncertainty in IL vapor pressure measurements. This weight factor helped the GlobalSearch method to find an accurate regression with low vapor pressure values. The pure component CPA parameters for [Emim][$MeSO_3$] and other compounds used in this work are shown in Table 7, while the resulting regressions for the [Emim][$MeSO_3$] parameters are presented in Fig. 2.

$$AARD\% = \frac{1}{n}\sum_{i}^{n}\left|\frac{x^{exp}-x^{cal}}{x^{exp}}\right|100\% \tag{10}$$

$$AAD = \frac{1}{n}\sum_{i}^{n}\left|x^{exp}-x^{cal}\right| \tag{11}$$

$$OF_1 = \sum_{i}^{n}\left(\frac{\rho_i^{exp}-\rho_i^{calc}}{\rho_i^{exp}}\right)^2 + 0.05\sum_{i}^{n}\left(\frac{P_i^{exp}-P_i^{calc}}{P_i^{exp}}\right)^2 \tag{12}$$

$$OF_2 = \sum_{i}^{n}\left(\frac{\rho_i^{exp}-\rho_i^{calc}}{\rho_i^{exp}}\right)^2 + \sum_{i}^{n}\left(\frac{C_{pi}^{exp}-C_{pi}^{calc}}{C_{pi}^{exp}}\right)^2 \tag{13}$$

where superscript calc and exp reference to calculated and experimental properties and ρ = density, P = vapor pressure, C_P=isobaric heat capacity. For calculating AAD, x^{exp} = experimentally studied property, x^{calc} = calculated property, and n = number of experimental points.

The performance of the CPAρP and CPAρC parameter sets in modelling pure component properties was compared. Each parameter set used density in the parameter regression. The CPAρC parameter set was more accurate for modelling density than the CPAρP parameter set, with AARD values of 0.2% and 1.5%, respectively. The temperature dependency in the CPAρP parameter set appeared damped, while the CPAρC parameters set followed it more accurately. The second used property in the parameter regression differed, the CPAρP parameter set used vapor pressure, whereas the CPAρC parameter set used isobaric heat capacity. The CPAρC parameter set was better than the CPAρP parameter set for modelling the isobaric heat capacity with AARD values of 0.04 % and 10.5 % AARD, respectively. From an application perspective, the difference between CPAρP and CPAρC parameter sets in modelling density is minimal and unlikely to have a significant impact on practical application. However, for isobaric heat capacity, the CPAρC parameter is expected to perform better, particularly in applications where the accuracy of heat capacity predictions is essential, such as heat transfer processes.

The most significant difference between these parameter sets was observed in their ability to model the vapor pressure of [Emim][$MeSO_3$].

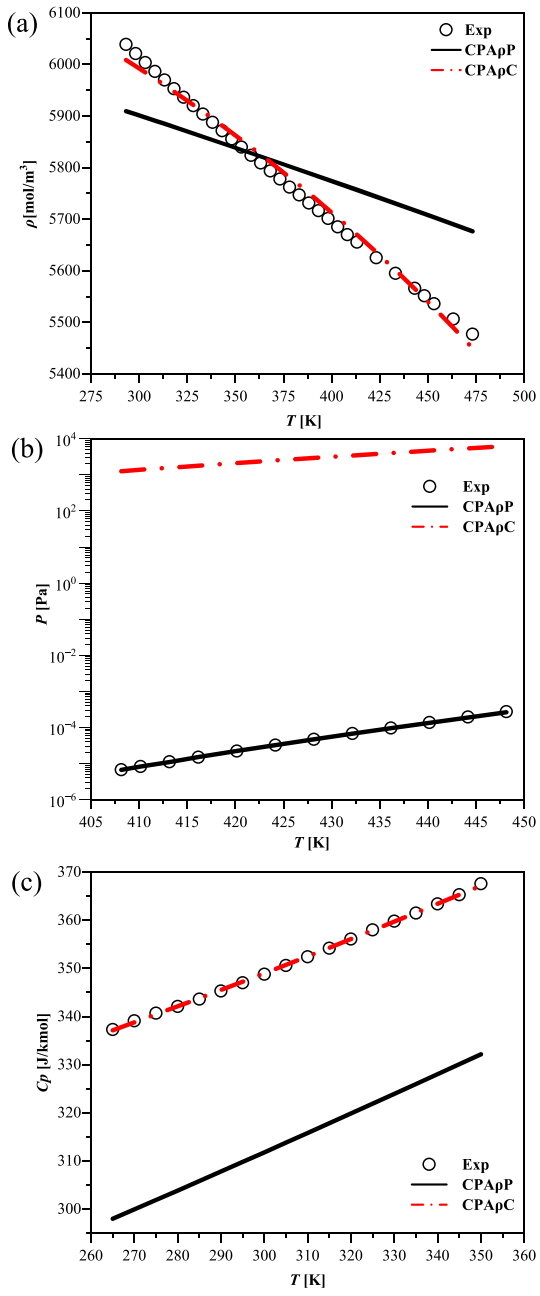

Fig. 2. CPA modelling of the [Emim][$MeSO_3$] pure component properties using the CPAρP and CPAρC parameter sets: (a) Density (data is shown in Table S2), (b) vapor pressure [52] and (c) isobaric heat capacity [53].

The CPAρP parameter set could accurately model the extremely low vapor pressure within 1.4 % AARD, while the CPAρC parameter set had a much higher AARD (see Table 7). This deviation between the CPAρP and CPAρC parameter sets is multiple orders of magnitude (10^{-4} vs 10^{4} Pa) (Fig. 2), and the high relative uncertainty (15 %) in the measured vapor

Table 7
The CPA pure component parameters, data type, and AARD% for parameter regression.

Compound scheme	Used data	b (cm^3/mol)	Γ (K)	c_1	β•1000	ε/R (K)	AARD ρ%	AARD P_{sat}%	AARD Cp%	Ref
[Emim][$MeSO_3$] 2B	ρ,P_{sat}	160.9	6828.888	0.5951	19.0	7505.763	1.4	1.4	10.5	This work
[Emim][$MeSO_3$] 2B	ρ,C	154.4	2713.743	1.4846	82.2	1007.491	0.2	$8.5{\cdot}10^9$	0.04	This work
H_2O 4C	ρ,P_{sat}	14.5	1018.334	0.6736	69.2	2003.136	0.5	0.8	n/a	[56]
MeOH 2B	ρ,P_{sat}	30.9	1577.591	0.4310	16.1	2957.782	0.5	0.6	n/a	[56]
DMC Non-associating	ρ,P_{sat}	73.1	2891.209	0.8937	-	-	0.5	0.8	n/a	[50]

Γ = reduced energy parameter ($a_0/b{\cdot}R$)

pressure of [Emim][$MeSO_3$] do not account for this large deviation. The differences in the modelling of [Emim][$MeSO_3$] vapor pressure between the CPAρP and CPAρC parameter sets highlight the importance of used properties in pure component parameter regression. The CPA model description about the [Emim][$MeSO_3$] differs significantly which can be seen from significantly different pure component parameter values. This might indicate that the model cannot identify some characteristics of the molecule when heat capacity is used, resulting high deviation for predicted [Emim][$MeSO_3$] vapor pressure. The realistic description about [Emim][$MeSO_3$] offers the possibility to realistically simulate the phase behavior, which can be used for designing the DMC synthesis.

The most noticeable difference between these parameter sets lies in the values of energy-related parameters (ε and Γ). The CPA model can achieve vapor pressure in the range of 10^{-4} Pa by significantly increasing the energy-related parameters. We also tested this effect with other ILs and observed a similar trend as with [Emim][$MeSO_3$], parameter regression with low vapor pressure data produced significantly higher ε or Γ values compared to regression using heat capacity and density (Tables S15 and S16). These elevated energy parameters suggest strong (roughly 3 times stronger than in methanol or water CPA parameter) ion-ion or association interactions and are also indicated by quantum chemical calculations [31]. These findings suggest that if vapor pressure data is not included in parameter regression, CPA might underestimate molecular interactions in [Emim][$MeSO_3$].

4.3. VLE and LLE modelling results for the binary mixtures

The VLE for H_2O + [Emim][$MeSO_3$] and MeOH + [Emim][$MeSO_3$] mixtures were modelled after regressing pure component parameters. TXY data used in modelling was measured in this work (Tables 4 and 5), while PXY data was obtained from the literature. The water content in the MeOH + [Emim][$MeSO_3$] mixture was considered at parameter regression. Both the CPAρP and CPAρC parameter sets were used in modelling and their performance was compared. The CPA can model phase equilibria with or without binary interaction parameter (k_{ij}), which is regressed from VLE data. We regressed the k_{ij} for both parameters set and compared the modelling results. The k_{ij} for binary VLE was regressed using OF_3 (Eq. (14)) and for LLE, using OF_4 (Eq. (15)). Table 8 and Fig. 3-5 show the performance of CPA with the CPAρP and CPAρC parameter sets, along with the fitted k_{ij} values for binary phase equilibria.

Table 8
CPA modelling results for VLE of H_2O + [Emim][$MeSO_3$] and MeOH + [Emim][$MeSO_3$] and LLE for DMC + [Emim][$MeSO_3$] mixtures by utilizing the CPAρP and CPAρC parameter sets and fitted k_{ij} values.

System	Parameter set	AAD T (K) $k_{ij}=0$	AAD P (kPa) or x_1^I $k_{ij}=0$	k_{ij}	AAD T (K)	AAD P (kPa) or x_1^I
H_2O-[Emim][$MeSO_3$]	CPAρP	29.2	12.0	-0.6284	3.8	2.3
H_2O-[Emim][$MeSO_3$]	CPAρC	31.7	14.3	-0.8468	5.2	2.6
MeOH-[Emim][$MeSO_3$]	CPAρP	9.0	10.9	-0.1885	2.3	0.4
MeOH-[Emim][$MeSO_3$]	CPAρC	8.5	10.6	-0.2374	2.6	0.8
DMC-[Emim][$MeSO_3$]	CPAρP	-	[a]	0.0246	-	0.01[b]
DMC-[Emim][$MeSO_3$]	CPAρC	-	[a]	0.0741	-	0.12[b]

a = LLE was not predicted for a full temperature range of experimental data.
b = AAD in x_1^I
x_1^I = DMC-rich liquid phase

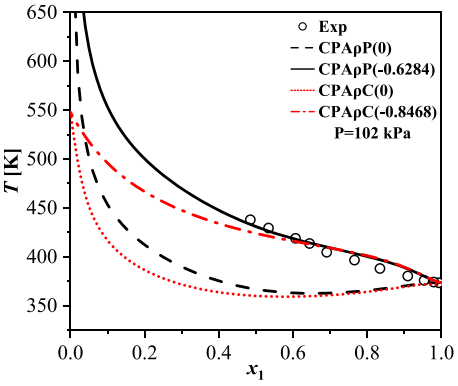

Fig. 3. TXY-diagram for H_2O (1) + [Emim][$MeSO_3$] (2) and CPA modelling results for the CPAρP and CPAρC parameter sets (k_{ij} are in parenthesis). Experimental data is shown in Table 4.

The CPAρP parameter set showed slightly higher accuracy than the CPAρC parameter set in modelling the boiling point temperature of the H_2O + [Emim][$MeSO_3$] mixture. The ADD values for boiling point temperature were 29.2 and 31.7 K for the CPAρP and CPAρC parameter sets, with k_{ij} set to 0. Correspondingly, the AAD values for boiling point pressure were 12 kPa for the CPAρP parameter set and 14.3 kPa for the CPAρC parameter set, both with k_{ij} equal to 0. In addition, the trends of the model predictions are significantly different when k_{ij} is 0 for both parameter sets. The boiling point temperature and pressure trends are opposite to the experimental data up to approximately 0.6 mole faction of H_2O.

The accuracy of both parameter sets was significantly higher when the k_{ij} was regressed. For the CPAρP parameter set, the value of the k_{ij} parameter was -0.62 and the AAD values for boiling point temperature and pressure were 3.8 K and 2.3 kPa. For the CPAρC parameter set, the value of k_{ij} was -0.84, and AAD values for boiling point temperature and pressure were 5.2 K and 2.6 kPa. Therefore, the CPAρP parameter set demonstrated higher accuracy in modelling phase equilibria for the H_2O + [Emim][$MeSO_3$] mixture, both with and without the use of k_{ij}, and had a lower k_{ij} value compared to the CPAρC parameter set.

$$OF_3 = \sum_i^n \left|\frac{T^{exp} - T^{cal}}{T^{exp}}\right| + \sum_i^n \left|\frac{P^{exp} - P^{cal}}{P^{exp}}\right| \quad (14)$$

$$OF_4 = \sum_i^n \left|\frac{x_1^{exp} - x_1^{cal}}{x_1^{exp}}\right| \quad (15)$$

where superscript calc and exp reference to calculated and experimental properties. T = bubble point temperature, P = bubble point pressure, and x_1 = mole fraction of [Emim][$MeSO_3$].

The VLE of the MeOH + [Emim][$MeSO_3$] mixture was modelled similarly to that H_2O + [Emim][$MeSO_3$] mixture. The TXY data is measured in this work while PXY is obtained from the literature. The performance of CPAρP and CPAρC parameter sets were compared and

the k_{ij} is regressed in the same way as in the case of H_2O + [Emim][$MeSO_3$] mixture. The modelling results and the values of regressed k_{ij} are shown in Table 8 and Fig. 5.

The CPAρP and CPAρC parameter sets showed nearly the same performance in modelling the VLE of MeOH + [Emim][$MeSO_3$] mixture. For the CPAρP and CPAρC parameter sets, the AAD values in modelling the boiling point temperature with $k_{ij}=0$ were 8.7 and 8.4 K, respectively. This is clearly more accurate than modelling the VLE of the H_2O + [Emim][$MeSO_3$] mixture with $k_{ij}=0$, which had AAD values of 29.2 K and 31.7 K for CPAρP and CPAρC parameter sets. The performance in modelling boiling point pressure with $k_{ij}=0$ showed AAD values of 10.9

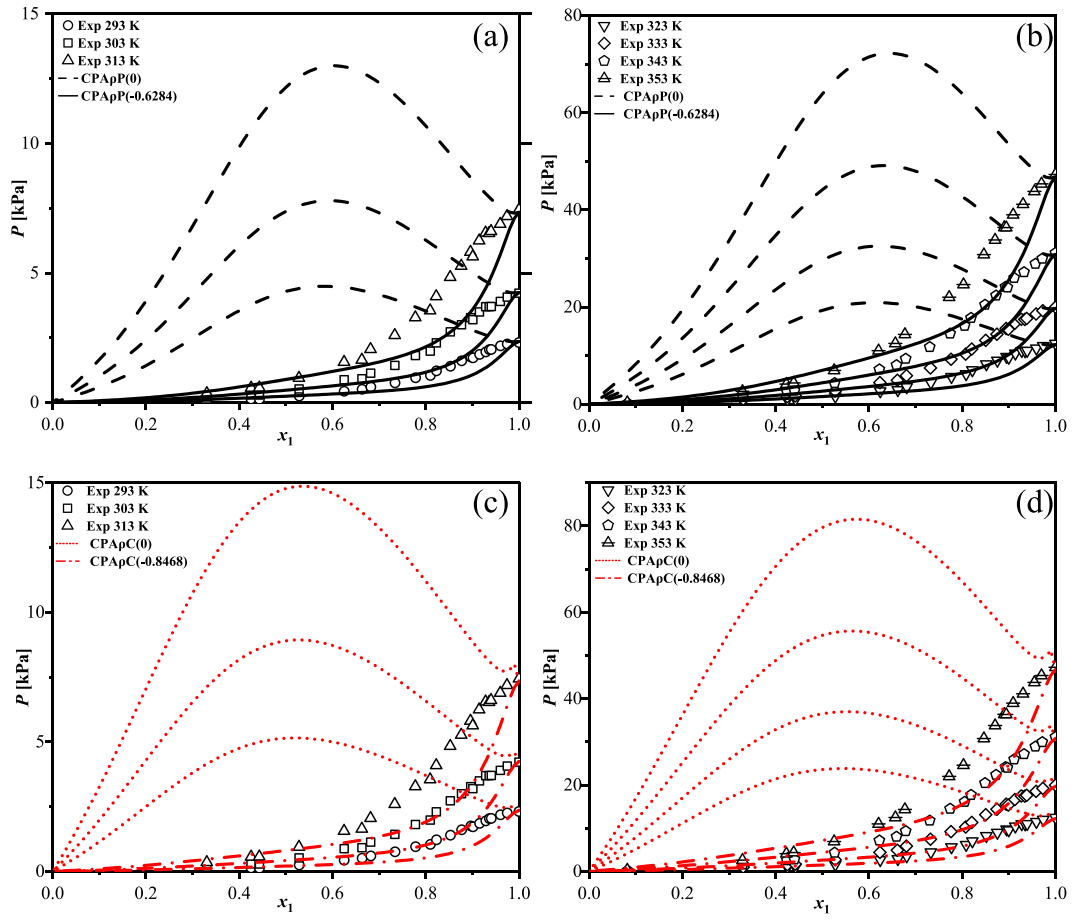

Fig. 4. PXY-diagram for H_2O (1) + [Emim][$MeSO_3$] (2) and CPA modelling results for the CPAρP and CPAρC parameter sets (k_{ij} are in parenthesis): (a) CPAρP at 293 – 313 K, (b) CPAρP at 323 – 353 K, (c) CPAρC at 293 – 313 K, (d) CPAρC 323 – 353 K. VLE data is taken from literature [57].

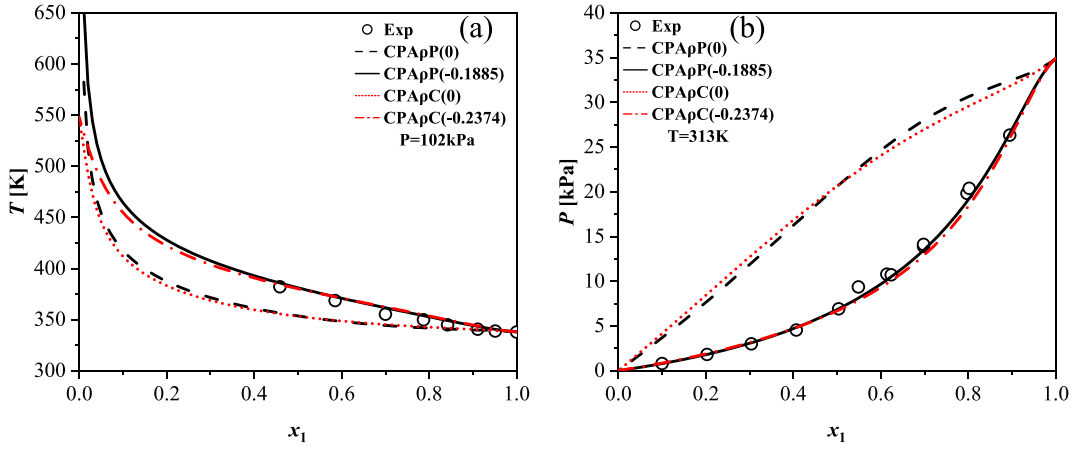

Fig. 5. MeOH (1) + [Emim][$MeSO_3$] (2) VLE and CPA modelling results for the CPAρP and CPAρC parameter sets (k_{ij} are in parenthesis): (a) TXY-diagram at 102 kPa (data is shown in Table 5), (b) PXY-diagram at 313 K (data is from literature [58]).

kPa and 10.6 kPa for the CPAρP and CPAρC parameter sets.

The values of k_{ij} were regressed using OF_3 from Eq. (14), resulting in k_{ij} values of -0.18 and -0.23 for the CPAρP and CPAρC parameter sets, respectively. With these regressed k_{ij} values, the accuracy in modelling the boiling point temperature improved. However, the difference between the CPAρP and CPAρC parameter sets could not be distinguished when fitted k_{ij} was used, since the performance of both parameter sets was within the uncertainty of the bubble point temperature measurement. The AAD values for the CPAρP and CPAρC parameter sets were 3.4 K and 3.6 K. Correspondingly, the accuracy in modelling boiling point pressure also improved when k_{ij} was fitted. The AAD values were 0.4 kPa and 0.8 kPa for the CPAρP and CPAρC parameter sets. Overall, the CPAρP parameter set demonstrated equivalent performance to the CPAρC parameter set in modelling the VLE of the MeOH + [Emim][$MeSO_3$] mixture.

Our experimental results showed that the DMC + [Emim][$MeSO_3$] mixture formed two liquid phases, therefore the LLE for this mixture was modelled. As with modelling binary VLE, the performance of the CPAρP

and CPAρC parameter sets was compared. both with and without regressing the k_{ij} parameter. The performance of both parameter sets along with the regressed k_{ij} values is presented in Table 8 and the LLE is shown in Fig. 6.

The CPA model did not predict any LLE for either parameter sets when the k_{ij} was set to 0. However, the LLE of the DMC + [Emim][$MeSO_3$] mixture was successfully modelled when the k_{ij} was regressed. The k_{ij} parameter was regressed by using Eq. (15), resulting the values of 0.024 and 0.074 for the CPAρP and CPAρC parameter sets, respectively. The CPAρP parameter set demonstrated higher accuracy in modelling the LLE. The values of AAD for the [Emim][$MeSO_3$] composition were 0.01 and 0.12 for the CPAρP and CPAρC parameter sets. These parameter sets with regressed k_{ij} values produced notably different LLE.

The CPAρP parameter set fitted well with the experimental data and predicted that liquid-liquid envelope to range from approximately 0.55 mole fraction DMC to practically pure DMC (0.999) mole fraction. In contracts, the CPAρC parameter set predicted that liquid-liquid envelope to range from around 0.3 mole fraction of DMC to approximately 0.98 mole fraction. However, the CPAρC parameter set fits poorly on the experimental data. Overall, the CPAρP parameter set was clearly more accurate in modelling the LLE for the DMC + [Emim][$MeSO_3$] mixture, while having a smaller absolute k_{ij} value.

4.4. VLE modelling results for the quaternary mixtures

The VLE of MeOH + DMC + H_2O + [Emim][$MeSO_3$] quaternary mixture was modelled using the CPAρP and CPAρC parameter sets, and their performance was compared. The k_{ij} parameter was regressed for [Emim][$MeSO_3$] + H_2O, + MeOH, + DMC binary mixtures in this work and the resulting k_{ij} values are shown in Table 8. The binary parameters for MeOH + DMC, H_2O + DMC, and H_2O + MeOH mixtures were obtained from the literature [50] and are shown in Table S17. The quaternary VLE data and the corresponding modelling results are presented in Fig.7-9. The performance of the CPAρP and CPAρC parameter sets in modelling the quaternary VLE is shown in Tables 9 and 10, as well as in Fig. 10.

In the quaternary VLE experiments, the mole fractions of the H_2O and [Emim][$MeSO_3$] remained approximately constant. Specifically, the mole fractions of H_2O were 0.1, 0.2, and 0.3, while those of [Emim][$MeSO_3$] were 0.05, 0.1, 0.2, and 0.3. These mole fraction variations influence the boiling point temperature and α_{12}. An increase in the mole fraction of H_2O results in a decrease in α_{12} values. For example, at a constant mole fraction of [Emim][$MeSO_3$] (0.05), the maximum experimental α_{12} values decreased from 2.1 to 1.3 as the mole fraction of H_2O increased from 0.1 to 0.3. Similarly, increasing the mole fraction of [Emim][$MeSO_3$] increased the boiling point temperature and α_{12}. For example, as shown in Fig. 7, at a mole fraction of [Emim][$MeSO_3$] of 0.05, the boiling point temperature ranged from 339.1 to 348.6 K, with corresponding α_{12} values ranging from 0.67 to 2.1. Similarly, at a higher mole fraction of [Emim][$MeSO_3$] (0.3), the boiling point temperature ranged from 353.3 K to 356.7 K, while corresponding α_{12} values ranged from 0.56 to 0.66. These trends revealed the contribution of different H_2O and [Emim][$MeSO_3$] compositions to α_{12} in complex quaternary

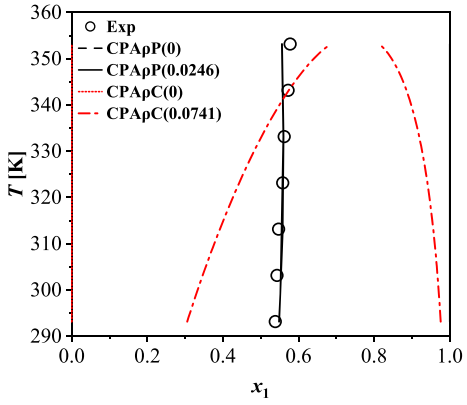

Fig. 6. DMC (1) + [Emim][$MeSO_3$] (2) LLE at 101.3 kPa and CPA modelling results for the CPAρP and CPAρC parameter sets (k_{ij} are in parenthesis). The LLE experimental results are presented in Table 6.

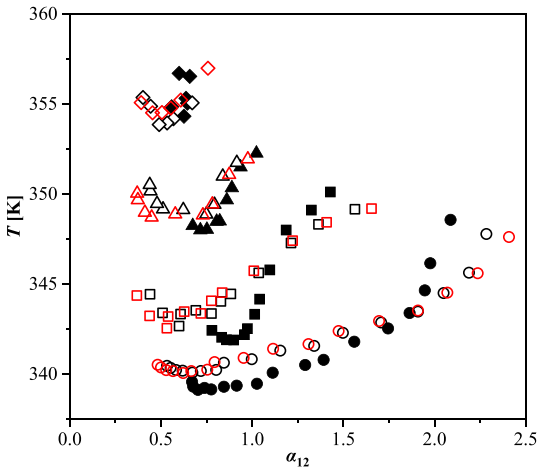

Fig. 7. Relative volatility of MeOH (α_{12}) at 102 kPa and CPA modelling results for the CPAρP and CPAρC parameter sets for different compositions. Pure component parameters are from Table 7 and binary interaction parameters k_{ij} are from Table 8 and Table S17. Experimental data is measured in this work and are shown in Tables S3-S14. Symbols: experiments; ●: $x_{H2O} \approx 0.1$ and $x_{[Emim][MeSO3]} \approx 0.05$, ■: $x_{H2O} \approx 0.1$ and $x_{[Emim][MeSO3]} \approx 0.1$, ▲: $x_{H2O} \approx 0.1$ and $x_{[Emim][MeSO3]} \approx 0.2$, ◆: $x_{H2O} \approx 0.1$ and $x_{[Emim][MeSO3]} \approx 0.3$. Modelling using CPAρP parameter set; ○: $x_{H2O} \approx 0.1$ and $x_{[Emim][MeSO3]} \approx 0.05$, □: $x_{H2O} \approx 0.1$ and $x_{[Emim][MeSO3]} \approx 0.1$, △: $x_{H2O} \approx 0.1$ and $x_{[Emim][MeSO3]} \approx 0.2$, ◇: $x_{H2O} \approx 0.1$ and $x_{[Emim][MeSO3]} \approx 0.3$. Modelling using CPAρC parameter set; ○: $x_{H2O} \approx 0.1$ and $x_{[Emim][MeSO3]} \approx 0.05$, □: $x_{H2O} \approx 0.1$ and $x_{[Emim][MeSO3]} \approx 0.1$, △: $x_{H2O} \approx 0.1$ and $x_{[Emim][MeSO3]} \approx 0.2$, ◇: $x_{H2O} \approx 0.1$ and $x_{[Emim][MeSO3]} \approx 0.3$.

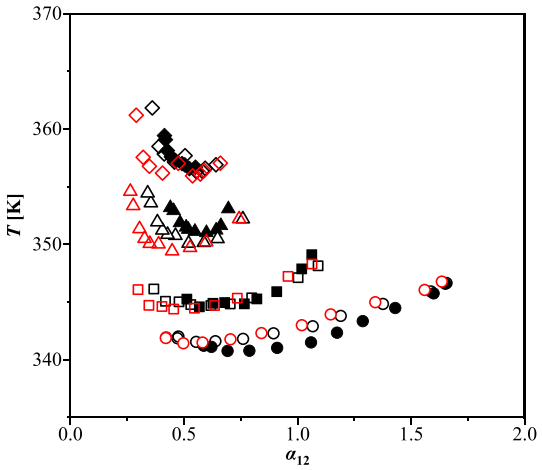

Fig. 8. Relative volatility of MeOH (α_{12}) at 102 kPa and CPA modelling results for the CPAρP and CPAρC parameter sets for different compositions. Pure component parameters are from Table 7 and binary interaction parameters k_{ij} are from Table 8 and Table S17. Experimental data is measured in this work and are shown in Tables S3-S14. Symbols: experiments; ●: $x_{H2O} \approx 0.2$ and $x_{[Emim][MeSO3]} \approx 0.05$, ■: $x_{H2O} \approx 0.2$ and $x_{[Emim][MeSO3]} \approx 0.1$, ▲: $x_{H2O} \approx 0.2$ and $x_{[Emim][MeSO3]} \approx 0.2$, ◆: $x_{H2O} \approx 0.2$ and $x_{[Emim][MeSO3]} \approx 0.3$. Modelling using CPAρP parameter set; ○: $x_{H2O} \approx 0.2$ and $x_{[Emim][MeSO3]} \approx 0.05$, □: $x_{H2O} \approx 0.2$ and $x_{[Emim][MeSO3]} \approx 0.1$, △: $x_{H2O} \approx 0.2$ and $x_{[Emim][MeSO3]} \approx 0.2$, ◇: $x_{H2O} \approx 0.2$ and $x_{[Emim][MeSO3]} \approx 0.3$. Modelling using CPAρC parameter set; ○: $x_{H2O} \approx 0.2$ and $x_{[Emim][MeSO3]} \approx 0.05$, □: $x_{H2O} \approx 0.2$ and $x_{[Emim][MeSO3]} \approx 0.1$, △: $x_{H2O} \approx 0.2$ and $x_{[Emim][MeSO3]} \approx 0.2$, ◇: $x_{H2O} \approx 0.2$ and $x_{[Emim][MeSO3]} \approx 0.3$.

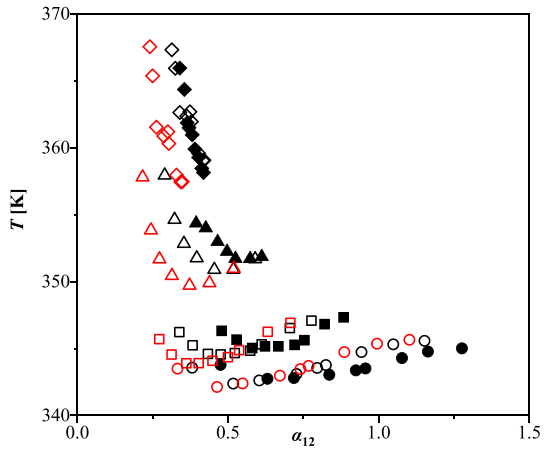

Fig. 9. Relative volatility of MeOH (α_{12}) at 102 kPa and CPA modelling results for the CPAρP and CPAρC parameter sets for different compositions. Pure component parameters are from Table 7 and binary interaction parameters k_{ij} are from Table 8 and Table S17. Experimental data is measured in this work and are shown in Tables S3-S14. Symbols: experiments; ●: $x_{H2O} \approx 0.3$ and $x_{[Emim][MeSO3]} \approx 0.05$, ■: $x_{H2O} \approx 0.3$ and $x_{[Emim][MeSO3]} \approx 0.1$, ▲: $x_{H2O} \approx 0.3$ and $x_{[Emim][MeSO3]} \approx 0.2$, ◆: $x_{H2O} \approx 0.3$ and $x_{[Emim][MeSO3]} \approx 0.3$. Modelling using CPAρP parameter set; ○: $x_{H2O} \approx 0.3$ and $x_{[Emim][MeSO3]} \approx 0.05$, □: $x_{H2O} \approx 0.3$ and $x_{[Emim][MeSO3]} \approx 0.1$, △: $x_{H2O} \approx 0.3$ and $x_{[Emim][MeSO3]} \approx 0.2$, ◇: $x_{H2O} \approx 0.3$ and $x_{[Emim][MeSO3]} \approx 0.3$. Modelling using CPAρC parameter set; ○: $x_{H2O} \approx 0.3$ and $x_{[Emim][MeSO3]} \approx 0.05$, □: $x_{H2O} \approx 0.3$ and $x_{[Emim][MeSO3]} \approx 0.1$, △: $x_{H2O} \approx 0.3$ and $x_{[Emim][MeSO3]} \approx 0.2$, ◇: $x_{H2O} \approx 0.3$ and $x_{[Emim][MeSO3]} \approx 0.3$.

Table 9
AAD values for bubble point temperature (T), MeOH vapor phase mole fraction (y_1), DMC vapor phase mole fraction (y_2), and relative volatility of methanol (α_{12}) between quaternary VLE of MeOH (1) + DMC (2) + H_2O (3) + [Emim][$MeSO_3$] (4) and CPA modelling results by using the CPAρP parameters set.

Mixture	AAD T (K)	AAD y_1	AAD y_2	AAD α_{12}
$x_3 \approx 0.1$ & $x_4 \approx 0.05$	0.74	0.01	0.02	0.12
$x_3 \approx 0.1$ & $x_4 \approx 0.1$	0.95	0.04	0.05	0.19
$x_3 \approx 0.1$ & $x_4 \approx 0.2$	1.11	0.05	0.07	0.19
$x_3 \approx 0.1$ & $x_4 \approx 0.3$	0.91	0.02	0.13	0.11
$x_3 \approx 0.2$ & $x_4 \approx 0.05$	0.57	0.02	0.02	0.10
$x_3 \approx 0.2$ & $x_4 \approx 0.1$	0.50	0.02	0.04	0.11
$x_3 \approx 0.2$ & $x_4 \approx 0.2$	0.71	0.03	0.03	0.08
$x_3 \approx 0.2$ & $x_4 \approx 0.3$	0.63	0.02	0.02	0.05
$x_3 \approx 0.3$ & $x_4 \approx 0.05$	0.31	0.03	0.03	0.12
$x_3 \approx 0.3$ & $x_4 \approx 0.1$	0.37	0.04	0.05	0.14
$x_3 \approx 0.3$ & $x_4 \approx 0.2$	0.95	0.03	0.04	0.08
$x_3 \approx 0.3$ & $x_4 \approx 0.3$	1.13	0.01	0.01	0.01
	0.74[a]	0.03[a]	0.04[a]	0.11[a]

a = average AAD calculated across all mixtures.

mixtures.

The performance of the CPAρP and CPAρC parameter sets was evaluated by comparing their accuracy in modelling the relative volatility of MeOH, boiling point temperature, mole fractions of MeOH, and DMC in the vapor phase. The quaternary mixture has more degrees of freedom compared to binary mixtures, so the AAD values were calculated both for each composition and for the entire set of compositions to ease the comparison. The AAD values for the CPAρP parameter set for relative volatility of MeOH, boiling point temperature, MeOH, and DMC vapor phase composition were 0.11, 0.74 K, 0.03, and 0.04. Similarly, the AAD values for the CPAρC parameter set for the same properties were 0.17, 0.85 K, 0.05, and 0.06. The accuracy in modelling of the quaternary VLE followed the same trend as observed in the case of binary VLE, where the CPAρP parameter set consistently demonstrated higher accuracy than the CPAρC parameter set.

Table 10
AAD values for bubble point temperature (T), MeOH vapor phase mole fraction (y_1), DMC vapor phase mole fraction (y_2), and relative volatility of methanol (α_{12}) between quaternary VLE MeOH (1), DMC (2), H_2O (3) and [Emim][$MeSO_3$] (4) and CPA modelling results by using the CPAρC parameters set.

Mixture	AAD T (K)	AAD y_1	AAD y_2	AAD α_{12}
$x_3 \approx 0.1$ & $x_4 \approx 0.05$	0.78	0.02	0.03	0.16
$x_3 \approx 0.1$ & $x_4 \approx 0.1$	0.88	0.05	0.06	0.26
$x_3 \approx 0.1$ & $x_4 \approx 0.2$	0.84	0.07	0.08	0.22
$x_3 \approx 0.1$ & $x_4 \approx 0.3$	0.64	0.05	0.04	0.11
$x_3 \approx 0.2$ & $x_4 \approx 0.05$	0.60	0.03	0.03	0.15
$x_3 \approx 0.2$ & $x_4 \approx 0.1$	0.53	0.05	0.06	0.25
$x_3 \approx 0.2$ & $x_4 \approx 0.2$	1.11	0.06	0.07	0.14
$x_3 \approx 0.2$ & $x_4 \approx 0.3$	0.97	0.03	0.04	0.07
$x_3 \approx 0.3$ & $x_4 \approx 0.05$	0.37	0.04	0.04	0.17
$x_3 \approx 0.3$ & $x_4 \approx 0.1$	0.87	0.07	0.08	0.21
$x_3 \approx 0.3$ & $x_4 \approx 0.2$	1.62	0.07	0.08	0.16
$x_3 \approx 0.3$ & $x_4 \approx 0.3$	0.95	0.05	0.05	0.09
	0.85[a]	0.05[a]	0.06[a]	0.17[a]

a = average AAD calculated across all mixtures.

5. Conclusion

This work focused on the phase equilibria of binary and quaternary mixtures containing the H_2O, MeOH, DMC, and [Emim][$MeSO_3$]. We measured the VLE for the binary mixtures of H_2O + [Emim][$MeSO_3$] and MeOH + [Emim][$MeSO_3$], and the LLE for DMC + [Emim][$MeSO_3$] mixture. Also, we investigated the impact of the exceptionally low vapor pressure (on the order of 10^{-4} Pa) of [Emim][$MeSO_3$] on phase equilibria modelling using the CPA. This provided insight into how this unique property influences the accuracy in modelling the phase equilibria. To model these systems, we regressed CPA pure component parameters for [Emim][$MeSO_3$] using two different approaches. In the first approach, we used density and saturated vapor pressure (CPAρP) while in the second approach, we used density and isobaric heat capacity (CPAρC).

The accuracy of CPAρP and CPAρC parameter sets was compared for modelling pure component properties. The CPAρP parameter set demonstrated AARD values of 1.4% and 10.6% for density and isobaric heat capacity, respectively. In contrast, the CPAρC parameter set showed 0.2% and 0.04% AARD values for density and isobaric heat capacity. However, the two parameter sets differed significantly in modelling the exceptionally low vapor pressure of [Emim][$MeSO_3$]. The CPAρP parameter set achieved significantly higher accuracy, with an AARD value of 1.4 %, while the CPAρC parameter set showed significantly larger deviation. The predicted vapor pressured for the CPAρP and CPAρC parameter sets were on the order of 10^{-4} and 10^{4} Pa, respectively.

The two parameter sets differed primarily in the energy-related parameters (ε and Γ). The CPAρP parameter set showed significantly higher energy-related parameters than CPAρC parameter set, indicating that including the exceptionally low vapor pressure of [Emim][$MeSO_3$] in the CPA pure component parameter regression enhances the accuracy in identifying the energy related parameters. This suggest that excluding vapor pressure data from the regression may lead CPA to underestimate the interactions within [Emim][$MeSO_3$].

The CPAρP parameter set showed consistently higher accuracy in modelling studied phase equilibria. For the [Emim][$MeSO_3$] + H_2O binary mixture, the CPAρP parameter set showed slightly better accuracy in modelling the VLE. However, the CPAρP parameter set achieved notably higher accuracy in modelling the LLE of [Emim][$MeSO_3$] + DMC mixture. The AAD values of [Emim][$MeSO_3$] liquid phase composition for the CPAρP and CPAρC parameter set were 0.01 and 0.12, respectively.

The performance of the CPAρP and CPAρC parameter sets was compared in modelling of the VLE of [Emim][$MeSO_3$] + H_2O + MeOH + DMC quaternary mixture. Many properties were studied from the quaternary mixtures such as relative volatility of MeOH, boiling point temperature, MeOH and DMC vapor phase composition. The CPAρP

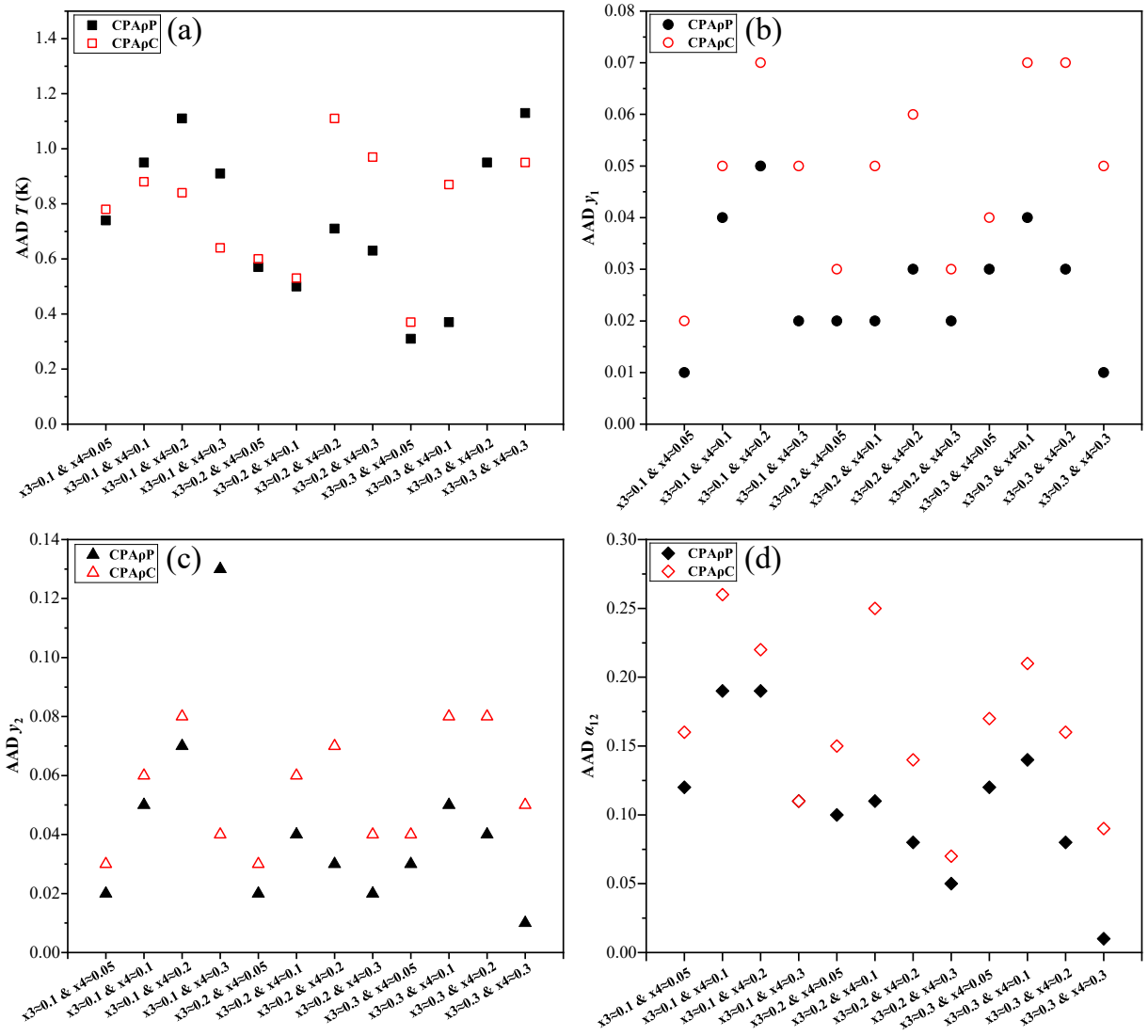

Fig. 10. AAD between quaternary VLE experimental data (Tables S3-S14) and CPA modelling results by using the CPAρP and CPAρC parameter sets for [Emim][$MeSO_3$]: (a) Bubble point temperature T, (b) MeOH vapor fraction y_1, (c) DMC vapor fraction y_2 and (d) relative volatility of methanol α_{12}.

parameter set demonstrated higher accuracy across all these properties, with AAD values for relative volatility of MeOH, boiling point temperature, MeOH and DMC vapor phase compositions were 0.11, 0.74 K, 0.03 and 0.04 respectively. In contrast, the CPAρC parameter set, showed AAD values of 0.17, 0.85 K, 0.05 and 0.06 for the same properties respectively.

The results of this work demonstrated that regressing CPA pure component parameters for [Emim][$MeSO_3$] by using CPAρP approach enhances the accuracy of phase equilibria modelling in binary and quaternary mixtures involving [Emim][$MeSO_3$], H_2O, MeOH, and DMC compared to CPAρC approach. This approach could improve the reliability of phase equilibria predictions for systems that contains ILs, which is crucial for applications where ILs are used.

CRediT authorship contribution statement

Juho-Pekka Laakso: Writing – review & editing, Writing – original draft, Investigation, Conceptualization. **Behnaz Asadzadeh:** Writing – review & editing, Investigation. **Petri Uusi-Kyyny:** Writing – review & editing, Supervision, Resources, Project administration. **Xiaodong Liang:** Writing – review & editing, Supervision, Software. **Georgios M. Kontogeorgis:** Writing – review & editing, Supervision. **Ville Alopaeus:** Writing – review & editing, Supervision, Resources, Project administration.

Declaration of competing interest

The authors declare that they have no known competing financial interests or personal relationships that could have appeared to influence the work reported in this paper.

Acknowledgments

This work was finically supported by the Academy of Finland 'In-situ equilibrium shifting in CO2 utilization reactions by novel absorbents (CO2Shift)' Project (351113).

Appendix A. Supplementary data

Supplementary data to this article can be found online at https://doi.org/10.1016/j.molliq.2024.126775.

Data availability

The data can be found on supplementary material

References

[1] B.A.V. Santos, V.M.T.M. Silva, J.M. Loureiro, A.E. Rodrigues, Review for the Direct Synthesis of Dimethyl Carbonate, ChemBioEng Reviews 1 (2014) 214–229, https://doi.org/10.1002/cben.201400020.

[2] D. Shi, S. Heyte, M. Capron, S. Paul, Catalytic processes for the direct synthesis of dimethyl carbonate from CO2and methanol: A review, Green Chemistry 24 (2022) 1067–1089, https://doi.org/10.1039/d1gc04093f.

[3] J.G. McDaniel, A. Verma, On the Miscibility and Immiscibility of Ionic Liquids and Water, Journal of Physical Chemistry B 123 (2019) 5343–5356, https://doi.org/10.1021/acs.jpcb.9b02187.

[4] M. Krannich, F. Heym, A. Jess, Characterization of Six Hygroscopic Ionic Liquids with Regard to Their Suitability for Gas Dehydration: Density, Viscosity, Thermal and Oxidative Stability, Vapor Pressure, Diffusion Coefficient, and Activity Coefficient of Water, J Chem Eng Data 61 (2016) 1162–1176, https://doi.org/10.1021/acs.jced.5b00806.

[5] C. Zheng, J. Zhou, Y. Pei, B. Yang, Equilibrium Thermodynamic Properties of Aqueous Solutions of Ionic Liquid 1-Ethyl-3-Methylimidazolium Methanesulfonate [EMIM][MeSO3, Sci Rep 10 (2020) 3174, https://doi.org/10.1038/s41598-020-59702-z.

[6] J.P. Hallett, T. Welton, Room-temperature ionic liquids: Solvents for synthesis and catalysis. 2, Chem Rev 111 (2011) 3508–3576, https://doi.org/10.1021/cr1003248.

[7] S.K. Singh, A.W. Savoy, Ionic liquids synthesis and applications: An overview, J Mol Liq 297 (2020), https://doi.org/10.1016/j.molliq.2019.112038.

[8] P. Halder, S. Kundu, S. Patel, A. Setiawan, R. Atkin, R. Parthasarthy, J. Paz-Ferreiro, A. Surapaneni, K. Shah, Progress on the pre-treatment of lignocellulosic biomass employing ionic liquids, Renewable and Sustainable Energy Reviews 105 (2019) 268–292, https://doi.org/10.1016/j.rser.2019.01.052.

[9] M. Aghaie, N. Rezaei, S. Zendehboudi, A systematic review on CO2 capture with ionic liquids: Current status and future prospects, Renewable and Sustainable Energy Reviews 96 (2018) 502–525, https://doi.org/10.1016/j.rser.2018.07.004.

[10] Y. Pei, Y. Zhang, J. Ma, M. Fan, S. Zhang, J. Wang, Ionic liquids for advanced materials, Mater Today Nano 17 (2022), https://doi.org/10.1016/j.mtnano.2021.100159.

[11] A.A. Quintana, A.M. Sztapka, V. de C. Santos Ebinuma, C. Agatemor, Enabling Sustainable Chemistry with Ionic Liquids and Deep Eutectic Solvents: A Fad or the Future? Angewandte Chemie - International Edition 61 (2022) https://doi.org/10.1002/anie.202205609.

[12] A. Stark, A.W. Zidell, M.M. Hoffmann, Is the ionic liquid 1-ethyl-3-methylimidazolium methanesulfonate [emim][MeSO3] capable of rigidly binding water? J Mol Liq 160 (2011) 166–179, https://doi.org/10.1016/j.molliq.2011.03.014.

[13] Z. Lei, J. Zhang, Q. Li, B. Chen, UNIFAC model for ionic liquids, Ind Eng Chem Res 48 (2009) 2697–2704, https://doi.org/10.1021/ie801496e.

[14] H. Renon, J.M. Prausnitz, Local Compositions in Thermodynamic Excess Functions for Liquid Mixtures, AIChE Journal 14 (1968) 135–144.

[15] Z.S. Baird, P. Uusi-Kyyny, J. Witos, A.H. Rantamäki, H. Sixta, S.K. Wiedmer, V. Alopaeus, Vapor-Liquid Equilibrium of Ionic Liquid 7-Methyl-1,5,7-triazabicyclo [4.4.0]dec-5-enium Acetate and Its Mixtures with Water, J Chem Eng Data 65 (2020) 2405–2421, https://doi.org/10.1021/acs.jced.9b01039.

[16] M. Diedenhofen, A. Klamt, COSMO-RS as a tool for property prediction of IL mixtures-A review, Fluid Phase Equilib 294 (2010) 31–38, https://doi.org/10.1016/j.fluid.2010.02.002.

[17] G.M. Kontogeorgis, E.C. Voutsas, I.V. Yakoumis, D.P. Tassios, An Equation of State for Associating Fluids, Ind Eng Chem Res 35 (1996) 4310–4318. https://pubs.acs.org/sharingguidelines.

[18] J. Gross, G. Sadowski, Perturbed-chain SAFT: An equation of state based on a perturbation theory for chain molecules, Ind Eng Chem Res 40 (2001) 1244–1260, https://doi.org/10.1021/ie0003887.

[19] G.M. Kontogeorgis, X. Liang, A. Arya, I. Tsivintzelis, Equations of state in three centuries. Are we closer to arriving to a single model for all applications? Chemical Engineering Science (2020) https://doi.org/10.1016/j.cesx.2020.100060. X 7.

[20] F.M. Maia, I. Tsivintzelis, O. Rodriguez, E.A. Macedo, G.M. Kontogeorgis, Equation of state modelling of systems with ionic liquids: Literature review and application with the Cubic Plus Association (CPA) model, Fluid Phase Equilib 332 (2012) 128–143, https://doi.org/10.1016/j.fluid.2012.06.026.

[21] Y. Wang, S. Huang, X. Liu, M. He, Thermodynamic model for CO2 absorption in imidazolium-based ionic liquids using cubic plus association equation of state, J Mol Liq 378 (2023), https://doi.org/10.1016/j.molliq.2023.121587.

[22] H. Passos, I. Khan, F. Mutelet, M.B. Oliveira, P.J. Carvalho, L.M.N.B.F. Santos, C. Held, G. Sadowski, M.G. Freire, J.A.P. Coutinho, Vapor-liquid equilibria of water + alkylimidazolium-based ionic liquids: Measurements and perturbed-chain statistical associating fluid theory modeling, Ind Eng Chem Res 53 (2014) 3737–3748, https://doi.org/10.1021/ie4041093.

[23] B. Maribo-Mogensen, K. Thomsen, G.M. Kontogeorgis, An electrolyte CPA equation of state for mixed solvent electrolytes, AIChE Journal 61 (2015) 2933–2950, https://doi.org/10.1002/aic.14829.

[24] L.F. Cameretti, G. Sadowski, J.M. Mollerup, Modeling of aqueous electrolyte solutions with perturbed-chain statistical associated fluid theory, Ind Eng Chem Res 44 (2005) 3355–3362, https://doi.org/10.1021/ie0488142.

[25] C. Held, T. Reschke, S. Mohammad, A. Luza, G. Sadowski, EPC-SAFT revised, Chemical Engineering Research and Design 92 (2014) 2884–2897, https://doi.org/10.1016/j.cherd.2014.05.017.

[26] L.A. Follegatti-Romero, X. Liang, Modelling thermophysical properties of mixtures of 2-hydroxyethyl ammonium-based ionic liquids + water, methanol, or ethanol with the electrolyte-cubic plus association equation of state, Fluid Phase Equilib 580 (2024), https://doi.org/10.1016/j.fluid.2024.114051.

[27] L. Sun, X. Liang, N. von Solms, G.M. Kontogeorgis, Modeling Tetra-n-butyl ammonium halides aqueous solutions with the electrolyte cubic plus association equation of state, Fluid Phase Equilib 486 (2019) 37–47, https://doi.org/10.1016/j.fluid.2018.12.033.

[28] X. Ji, C. Held, G. Sadowski, Modeling imidazolium-based ionic liquids with ePC-SAFT, Fluid Phase Equilib 335 (2012) 64–73, https://doi.org/10.1016/j.fluid.2012.05.029.

[29] X. Liao, K. Zheng, G. Wang, Y. Yang, Y. Li, M.O. Coppens, Solubility of CO2 in Ionic Liquids with Additional Water and Methanol: Modeling with PC-SAFT Equation of State, Ind Eng Chem Res 61 (2022) 14364–14373, https://doi.org/10.1021/acs.iecr.2c02778.

[30] K. Ueno, H. Tokuda, M. Watanabe, Ionicity in ionic liquids: correlation with ionic structure and physicochemical properties, Physical Chemistry Chemical Physics 12 (2010) 1648, https://doi.org/10.1039/c001176m.

[31] P.A. Hunt, C.R. Ashworth, R.P. Matthews, Hydrogen bonding in ionic liquids, Chem Soc Rev 44 (2015) 1257–1288, https://doi.org/10.1039/c4cs00278d.

[32] K. Paduszyński, U. Domańska, Thermodynamic modeling of ionic liquid systems: Development and detailed overview of novel methodology based on the PC-SAFT, Journal of Physical Chemistry B 116 (2012) 5002–5018, https://doi.org/10.1021/jp3009207.

[33] S.H. Huang, M. Radosz, Equation of State for Small, Large, Polydisperse, and Associating Molecules, Ind. Eng. Chem. Res 29 (1990) 2284–2294. https://pubs.acs.org/sharingguidelines.

[34] G.M. Kontogeorgis, G.K. Folas, Thermodynamic Models for Industrial Applications: From Classical and Advanced Mixing Rules to Association Theories, John Wiley & Sons, 2010.

[35] C. Zhu, M. He, X. Liu, G.M. Kontogeorgis, X. Liang, Quantification of Dipolar Contribution and Modeling of Green Polar Fluids with the Polar Cubic-Plus-Association Equation of State, ACS Sustain Chem Eng 9 (2021) 7602–7619, https://doi.org/10.1021/acssuschemeng.1c01545.

[36] K. Paduszyński, Thermodynamic Modeling of Multicomponent Liquid-Liquid Equilibria in Ionic Liquid Systems with PC-SAFT Equation of State, Ind Eng Chem Res 57 (2018) 5413–5432, https://doi.org/10.1021/acs.iecr.8b00175.

[37] L.F. Vega, F. Llovell, Review and new insights into the application of molecular-based equations of state to water and aqueous solutions, Fluid Phase Equilib 416 (2016) 150–173, https://doi.org/10.1016/j.fluid.2016.01.024.

[38] G.M. Kontogeorgis, M.L. Michelsen, G.K. Folas, S. Derawi, N. Von Solms, E. H. Stenby, Ten Years with the CPA (Cubic-Plus-Association) equation of state. Part 1. Pure compounds and self-associating systems, Ind Eng Chem Res 45 (2006) 4855–4868, https://doi.org/10.1021/ie051305v.

[39] R.M. Frias, L.M. Follegatti-Romero, L.A. Follegatti-Romero, Modelling mixtures of ammonium and pyridinium-based ionic liquids and carbon dioxide with the Cubic Plus Association Equation of state, Fluid Phase Equilib 574 (2023), https://doi.org/10.1016/j.fluid.2023.113910.

[40] K. Paduszyński, M. Okuniewski, U. Domańska, Renewable feedstocks in green solvents: Thermodynamic study on phase diagrams of d-sorbitol and xylitol with dicyanamide based ionic liquids, Journal of Physical Chemistry B 117 (2013) 7034–7046, https://doi.org/10.1021/jp401937p.

[41] S. Yerazunis, J.D. Plowright, F.M. Smola, Vapor-liquid equilibrium determination by a new apparatus, AIChE Journal 10 (1964) 660–665, https://doi.org/10.1002/aic.690100517.

[42] P. Uusi-Kyyny, J.P. Pokki, J. Aittamaa, S. Liukkonen, Vapor-liquid equilibrium for the binary systems of 3-methylpentane + 2-methyl-2-propanol at 331 K and + 2-butanol at 331 K, J Chem Eng Data 46 (2001) 754–758, https://doi.org/10.1021/je000295w.

[43] Working Group 1 of the Joint Committee for Guides in Metrology (JCGM/WG 1), JCGM 100 2008 GUM 1995 with minor correction. Evaluation of measurement data Guide to the expression of uncertainty in measurement, 2008., n.d. https://www.bipm.org/utils/common/documents/jcgm/JCGM_100_2008_E.pdf (accessed August 5, 2024).

[44] R. Dahal, P. Uusi-Kyyny, J.P. Pokki, V. Alopaeus, Liquid – liquid equilibria in binary and ternary systems of phenol + hydrocarbons (n–dodecane or n–hexadecane) and water + phenol + hydrocarbons (n–dodecane or n–hexadecane) at temperatures between 298K and 353K, Fluid Phase Equilib 556 (2022), https://doi.org/10.1016/j.fluid.2022.113402.

[45] R.D. Chirico, M. Frenkel, J.W. Magee, V. Diky, C.D. Muzny, A.F. Kazakov, K. Kroenlein, I. Abdulagatov, G.R. Hardin, W.E. Acree, J.F. Brenneke, P.L. Brown, P.T. Cummings, T.W. De Loos, D.G. Friend, A.R.H. Goodwin, L.D. Hansen, W. M. Haynes, N. Koga, A. Mandelis, K.N. Marsh, P.M. Mathias, C. McCabe, J. P. O'Connell, A. Pádua, V. Rives, C. Schick, J.P.M. Trusler, S. Vyazovkin, R.D. Weir, J. Wu, Improvement of quality in publication of experimental thermophysical property data: Challenges, assessment tools, global implementation, and online support, J Chem Eng Data 58 (2013) 2699–2716, https://doi.org/10.1021/je400569s.

[46] G. Soave, Equilibrium constants from a modified Redlich-Kwong equation of state, Chem Eng Sci 27 (1972) 1197–1203.

[47] Q. Li, S. Zhang, B. Ding, L. Cao, P. Liu, Z. Jiang, B. Wang, Isobaric vapor-liquid equilibrium for methanol + dimethyl carbonate + trifluoromethanesulfonate-

based ionic liquids at 101.3 kPa, J Chem Eng Data 59 (2014) 3488–3494, https://doi.org/10.1021/je500443v.
[48] C. Du, Z. Du, B. Long, H. Du, Z. Yan, X. Yin, Isobaric Vapor-Liquid Equilibria of Binary Mixtures of Diethyl Carbonate with Methyl Acetate, n-Propyl Acetate, or Amyl Acetate at 100.17 kPa, J Chem Eng Data 64 (2019) 2550–2557, https://doi.org/10.1021/acs.jced.9b00068.
[49] J.W. Kang, V. Diky, R.D. Chirico, J.W. Magee, C.D. Muzny, I. Abdulagatov, A. F. Kazakov, M. Frenkel, Quality assessment algorithm for vapor-liquid equilibrium data, J Chem Eng Data 55 (2010) 3631–3640, https://doi.org/10.1021/je1002169.
[50] I. Tsivintzelis, N.E. Musko, A. Baiker, J.D. Grunwaldt, G.M. Kontogeorgis, Experimental determination and modeling of the phase behavior for the direct synthesis of dimethyl carbonate from methanol and carbon dioxide, Journal of Supercritical Fluids 84 (2013) 155–163, https://doi.org/10.1016/j.supflu.2013.09.020.
[51] M.S. Manic, A.J. Queimada, E.A. MacEdo, V. Najdanovic-Visak, High-pressure solubilities of carbon dioxide in ionic liquids based on bis(trifluoromethylsulfonyl) imide and chloride, Journal of Supercritical Fluids 65 (2012) 1–10, https://doi.org/10.1016/j.supflu.2012.02.016.
[52] F. Heym, W. Korth, B.J.M. Etzold, C. Kern, A. Jess, Determination of vapor pressure and thermal decomposition using thermogravimetrical analysis, Thermochim Acta 622 (2015) 9–17, https://doi.org/10.1016/j.tca.2015.03.020.
[53] V. Štejfa, J. Rohlíček, C. Červinka, Phase behaviour and heat capacities of selected 1-ethyl-3-methylimidazolium-based ionic liquids II, Journal of Chemical Thermodynamics 160 (2021), https://doi.org/10.1016/j.jct.2021.106392.
[54] Optimization Toolbox,version 23.2 (R2023b), Natick, Massachusetts: The MathWorks Inc.; 2023, (n.d.).
[55] J.O. Valderrama, P.A. Robles, Critical properties, normal boiling temperatures, and acentric factors of fifty ionic liquids, Ind Eng Chem Res 46 (2007) 1338–1344, https://doi.org/10.1021/ie0603058.
[56] G.K. Folas, G.M. Kontogeorgis, M.L. Michelsen, E.H. Stenby, Application of the cubic-plus-association (CPA) equation of state to complex mixtures with aromatic hydrocarbons, Ind Eng Chem Res 45 (2006) 1527–1538, https://doi.org/10.1021/ie050976q.
[57] N. Merkel, C. Weber, M. Faust, K. Schaber, Influence of anion and cation on the vapor pressure of binary mixtures of water+ionic liquid and on the thermal stability of the ionic liquid, Fluid Phase Equilib 394 (2015) 29–37, https://doi.org/10.1016/j.fluid.2015.03.001.
[58] J.M. Winnert, V.K.P.J. Devi, J.F. Brennecke, Using Dialkylimidazolium Ionic Liquids to Break the Methanol + Methyl Acetate Azeotrope, Ind Eng Chem Res 58 (2019) 22633–22639, https://doi.org/10.1021/acs.iecr.9b05760.